Journal of Medicinal Chemistry

Article

Structural Basis of Inhibitor Specificity of the Human Protooncogene Proviral Insertion Site in Moloney Murine Leukemia Virus (PIM-1) Kinase

Alex N. Bullock, Judit . Debreczeni, Oleg Y. Fedorov, Adam Nelson, Brian D. Marsden, and Stefan Knapp

J. Med. Chem., **2005**, 48 (24), 7604-7614• DOI: 10.1021/jm0504858 • Publication Date (Web): 27 October 2005

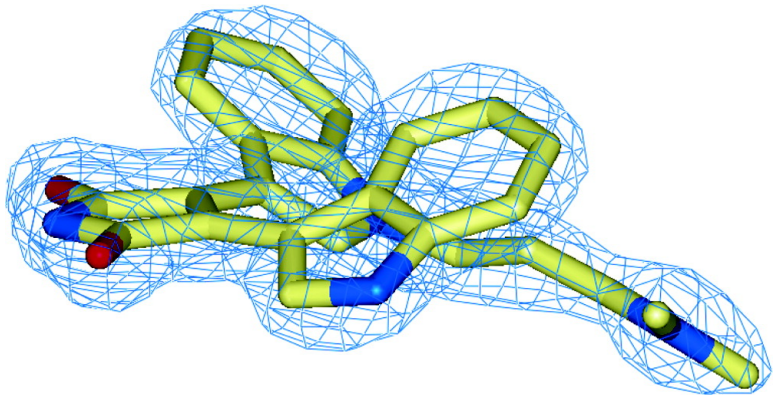

More About This Article

Additional resources and features associated with this article are available within the HTML version:

- Supporting Information
- Links to the 6 articles that cite this article, as of the time of this article download
- Access to high resolution figures
- Links to articles and content related to this article
- Copyright permission to reproduce figures and/or text from this article

View the Full Text HTML

Journal of Medicinal Chemistry is published by the American Chemical Society. 1155 Sixteenth Street N.W., Washington, DC 20036

Structural Basis of Inhibitor Specificity of the Human Protooncogene Proviral Insertion Site in Moloney Murine Leukemia Virus (PIM-1) Kinase

Alex N. Bullock,[†,‡] Judit É. Debreczeni,[†,‡] Oleg Y. Fedorov,[†,‡] Adam Nelson,[‡,§] Brian D. Marsden,[†,‡] and Stefan Knapp*[,†]

Structural Genomics Consortium (SGC), Botnar Research Centre, Oxford University, Oxford OX3 7LD, U.K., and School of Chemistry, University of Leeds, Leeds, LS2 9JT, U.K.

Received May 24, 2005

The kinase PIM-1 plays a pivotal role in cytokine signaling and is implicated in the development of a number of tumors. The three-dimensional structure of PIM-1 is characterized by an unique hinge region which lacks a second hydrogen bond donor and makes it particularly important to determine how inhibitors bind to this kinase. We determined the structures of PIM-1 in complex with bisindolylmaleimide (BIM-1) and established the structure−activity relationship (SAR) for this inhibitor class. In addition, we screened a kinase targeted library and identified a number of high affinity inhibitors of PIM-1 such as imidazo[1,2-*b*]pyridazines, pyrazolo[1,5-*a*]pyrimidines, and members of the flavonoid family. In this paper we present an initial SAR of the identified scaffolds determined on the basis of a thermostability shift assay, calorimetric binding data, and biochemical assays which may find applications for the treatment of PIM-1 dependent cancer types.

Introduction

The protooncogene PIM-1 kinase was first discovered as a preferential proviral insertion site in Moloney murine leukemia virus (MoMuLV) induced T-cell lymphoma.[1] Further studies showed that PIM-1 encodes for a highly conserved serine/threonine kinase which is mainly expressed in thymus, testis, and cells of the hematopoietic system.[2,3] PIM-1 expression is directly induced by STAT transcription factors,[4] and PIM-1 has therefore been implicated as an effector of many cytokine signaling pathways such as interleukins (IL), granulocyte-macrophage colony stimulating factor (GM-CSF), α- and γ-interferon, erythropoietin, and prolactin.[5] Recent data show that PIM-1 also stabilizes the negative regulator of the JAK/STAT pathway SOCS-1 by phosphorylation, suggesting that PIM-1 modulates a negative feedback mechanism in these cytokine signaling pathways.[6,7] Mice deficient for all three PIM genes showed an impaired response to hematopoietic growth factors and demonstrated that PIM proteins are required for efficient proliferation of peripheral T lymphocyes. In particular it was shown that PIM function is required for efficient cell cycle induction of T cells in response to synergistic T-cell receptor and IL-2 signaling.[2] A large number of interaction partners and substrates of PIM-1 have been identified,[5] suggesting a pivotal role for PIM-1 in cell cycle control, proliferation as well as in cell survival.

The oncogenic potential of this kinase has been first demonstrated in Eμ PIM-1 transgenic mice in which PIM-1 overexpression is targeted to the B-cell lineage which leads to formation of B-cell tumors.[8] Subsequently PIM-1 has been reported to be overexpressed in a number of prostate cancers, erythroleukemias, and several other types of human leukemias.[9−11] For example, chromosomal translocation of PIM-1 leads to overexpression of PIM-1 in diffuse large cell lymphoma.[12] Furthermore, a number of missense mutations in PIM-1 have been reported in lymphomas of the nervous system and AIDS-induced non-Hodgkins's lymphomas that probably affect PIM-1 kinase activity or stability.[13−15] Thus, the strong linkage between reported overexpression data and the occurrence of PIM-1 mutations in cancer suggests a dominant role of PIM-1 in tumorigenesis.

Several crystal structures of PIM-1 have been reported recently.[16−18] Interestingly, the presence of a proline residue in the hinge region of PIM-1 allows only for the formation of one hydrogen bond to the adenosine ring of ATP and so far makes the PIM family of kinases unique in the way they recognize ATP and consequently ATP mimetic inhibitors.[16]

In order to identify inhibitor scaffolds for PIM-1 we screened a small kinase targeted library of about 200 compounds and determined the structure−activity relationship (SAR) for commercially available analogues of the identified scaffolds. In this report we identified members of the kinase inhibitor family of bisindolylmaleimides (BIM) as very potent inhibitors of PIM-1 and determined the cocrystal structure of BIM-1 with the nonphosphorylated and phosphorylated PIM-1. The bisindolylmaleimide scaffold is based on the nonspecific kinase inhibitor staurosporine.[19] Members of this class were originally reported as selective PKC inhibitors.[20,21] A related inhibitor **1** (LY333531) has been developed for the specific inhibition of PKCβ and is currently in phase III clinical trials for the treatment of left ventricular hypertrophy in heart failure as well as for diabetes complications such as diabetic retinopathy.[22]

* To whom correspondence should be addressed. Tel.: + 44 1865 227978. Fax: + 44 1865 737231. E-mail: stefan.knapp@sgc.ox.ac.uk.
† Oxford University.
‡ E-mail: alex.bullock@sgc.ox.ac.uk, judit.debreczeni@sgc.ox.ac.uk, oleg.fedorov@sgc.ox.ac.uk, a.s.nelson@leeds.ac.uk, brian.marsden@sgc.ox.ac.uk.
§ University of Leeds.

10.1021/jm0504858 CCC: $30.25
Published on Web 10/27/2005

In addition, we identified several flavonoids, imidazo[1,2-*b*]pyridazines, and pyrazolo[1,5-*a*]pyrimidines as potent inhibitors of PIM-1. Analysis of the determined high-resolution structural data of the BIM-1 complex with PIM-1 kinase as well as the determined SAR gives interesting insight into the recognition of the identified inhibitors and suggests applications of these well-studied compounds for the treatment of leukemia and other PIM-1 dependent cancer types.

Material and Methods

Compounds. BIM-4 was purchased from ALEXIS. Staurosporine, BIM-8, BIM-9, BIM-10, and BIM-11 were purchased from LC laboratories. BIM-A, BIM-B, BIM-C, BIM-D, and BIM-E were synthesized as described previously.[23] Fisetin, luteolin, kaempferol, chrysin, baicalein, biochanin A, and myricetin were purchased from Sigma Aldrich. Chromene-3,4-dione 1 (5,7-dihydroxy-2-(3,4,5-trihydroxyphenyl)-2*H*-chromene-3,4-dione) was purchased from InterBioScreen, compound ID STOCK1N-00524. Chromene-3,4-dione 2 (5,7-dihydroxy-2-(4-hydroxy-3-methoxyphenyl)-2*H*-chromene-3,4-dione) was purchased from InterBioScreen, compound ID STOCK1N-00608. Chromene-3,4-dione 3 (2-(3,4-dihydroxyphenyl)-5,7-dihydroxy-8-methyl-2*H*-chromene-3,4-dione) was purchased from Nanosyn, compound ID NS64156. Chromene-3,4-dione 4 (5,7-dihydroxy-2-(4-hydroxyphenyl)-2*H*-chromene-3,4-dione) was purchased from Nanosyn, compound ID NS64159. Chromene-3,4-dione 5 (2-(2,4-dihydroxyphenyl)-5,7-dihydroxy-2*H*-chromene-3,4-dione) was purchased from InterBioScreen, compound ID STOCK1N-05787. Chromene-3,4-dione 6 (2-(3-hydroxyphenyl)-2*H*-chromene-3,4-dione) was purchased from TimTec Inc, compound ID ST055991. Chromene-3,4-dione 7 (6-hydroxy-2-phenyl-2*H*-chromene-3,4-dione) was purchased from InterBioScreen, compound ID STOCK1N-04756. Chromene-3,4-dione 8 (2-(3,4-dimethoxyphenyl)-6-methyl-2*H*-chromene-3,4-dione) was purchased from TimTec Inc, compound ID ST056253. Chromene-3,4-dione 9 (2-(4-methylphenyl)-2*H*-chromene-3,4-dione) was purchased from InterBioScreen, compound ID STOCK1S-88260. Imidazo[1,2-*b*]pyridazine **1** (1-(3-{6-[(cyclopropylmethyl)amino]imidazo[1,2-*b*]pyridazin-3-yl}phenyl)ethanone) was purchased from BioFocus, compound ID 229_4051_4145). Imidazo[1,2-*b*]pyridazine 2 (3-(3-chlorophenyl)-*N*-tetrahydro-2*H*-pyran-4-ylimidazo[1,2-*b*]pyridazin-6-amine) was purchased from BioFocus, compound ID 229_0242_0279. Imidazo[1,2-*b*]pyridazine 3 (3-(3-chlorophenyl)-*N*-(2-pyridin-2-ylethyl) imidazo[1,2-*b*]pyridazin-6-amine) was purchased from BioFocus, compound ID 229_0115_0279. Imidazo[1,2-*b*]pyridazine 4 (3-phenyl-*N*-(thien-2-ylmethyl)imidazo[1,2-*b*]pyridazin-6-amine) was purchased from BioFocus, compound ID 229_0146_0061. Imidazo[1,2-*b*]pyridazine 5 (*N*-(4-fluorobenzyl)-3-(2-furyl)imidazo[1,2-*b*]pyridazin-6-amine) was purchased from BioFocus, compound ID 229_0224_0142. Imidazo[1,2-*b*]pyridazine 6 (*N*-(cyclopropylmethyl)-3-thien-2-ylimidazo[1,2-*b*]pyridazin-6-amine) was purchased from BioFocus, compound ID 229_4051_4147. Pyrazolo[1,5-*a*]pyrimidine 1 (3-(4-chlorophenyl)-*N*-(pyridin-3-ylmethyl)pyrazolo[1,5-*a*]pyrimidin-5-amine) was purchased from BioFocus, compound ID 294_4003_0160. All other compounds were purchased from Calbiochem.

Protein Expression and Purification. Full-length human PIM-1 (gi|33304198) was subcloned by ligation independent cloning into a pET-derived expression vector, pLIC, and expression performed in BL21(DE3) with 1 mM IPTG induction for 4 h at 18 °C. Cells were lysed using a high pressure homogenizer, cleared by centrifugation and the lysate purified by Ni-NTA chromatography. The eluted PIM-1 protein was treated with lambda phosphatase together with TEV protease overnight to remove phosphorylation and the hexa-histidine tag, respectively. The protein was further purified on a monoQ column and resolved into two species, shown by ESI-MS to be homogeneous nonphosphorylated and singularly phosphorylated PIM-1. These samples were concentrated to 10 mg/mL in the elution buffer, 50 mM HEPES pH 7.5, 250 mM NaCl, 5% glycerol, and 10 mM DTT.

Isothermal Titration Calorimetry (ITC). Calorimetric measurements were carried out using a VP-ITC titration calorimeter (MicroCal Inc). PIM-1 protein (100 to 150 μM) was dialyzed against 50 mM HEPES pH 7.5, 150 mM NaCl, and 1 mM DTT, and the identical buffer was used to dissolve the ligands (5 to 10 μM). Data were analyzed using a single binding site model implemented in the Origin software package provided with the instrument.

Kinase Assay. Phosphorylation reactions were monitored using a coupled-enzyme assay in which ADP production was coupled to NADH oxidation by pyruvate kinase (PK) and lactate dehydrogenase (LDH).[24] The assay was carried out in a total volume of 100 μL in a buffer containing 50 mM HEPES pH 7.5, 100 mM NaCl, 10 mM $MgCl_2$, 1.0 mM phosphoenolpyruvate, 0.1 mM NADH, 30 μg/mL pyruvate kinase, 10 μg/mL lactate dehydrogenase, and 20 nM PIM-1. The reaction was monitored at 340 nm at 25 °C on a Spectramax spectrophotometer (Molecular Devices, Sunnyvale, CA). The reaction was started by addition of ATP after a 10 min preincubation of the reaction mixture at 25 °C. Substrate concentrations were 30 μM using a recognition peptide of the PIM-1 substrate p21 (RKRRQTSMTD). The ATP concentration was 100 μM. Inhibitors, dissolved in DMSO, were added at the beginning of the preincubation period, resulting in a final DMSO concentration of 2% in the assay. Kinetic analysis was performed by nonlinear regression fitting using the program KaleidaGraph (SynergySoftware,CA).

Thermal Stability Measurements. Thermal melting experiments were carried out using a high temperature fluorescence microplate reader (FluoDia T70, Photon Tech. Int.). PIM-1 was buffered in 20 mM PIPES pH 7.0, 150 mM NaCl and assayed in a 96 well plate at a final concentration of 2 μM. Inhibitors were added at a final concentration of 10 μM from 500 μM stocks in DMSO. SYPRO-Orange (Molecular probes, OR) was added as a fluorescence probe at a dilution of 1 in 1000. The plate was shaken gently for 15 min at room temperature before starting the experiment. Excitation and emission filters for the SYPRO-Orange dye were set to 465 and 590 nm, respectively. Temperature was raised with a step of 1 °C per 1.5 min from 20 °C to 72 °C, and fluorescence readings were taken at each interval. The temperature dependence of the fluorescence during the protein denaturation process was approximated by the equation

$$y(T) = y_F + \frac{y_U - y_F}{1 + e^{\Delta uG_{(T)}/RT}}$$

where y_F and y_U are the fluorescence intensity of the probe in the presence of completely folded and unfolded protein, respectively.[25] The sloping baselines of these initial and final fluorescent species with increasing temperature were approximated by a linear fit. The observed temperature shifts, ΔT_m^{obs}, for each inhibitor were recorded as the difference between the transition midpoints of sample and reference wells containing protein without inhibitor in the same plate.

Crystallization. BIM-1 (2-[1-(3-dimethylaminopropyl)-1*H*-indol-3-yl]-3-(1*H*-indol-3-yl) maleimide, HCl) was purchased from Calbiochem and added at a concentration of 1 mM from a 50 mM DMSO stock solution to the protein. Nonphosphorylated PIM-1 crystals were grown at 4 °C in 3 μL sitting drops mixing 2.0 μL PIM-1 (10 mg/mL in 50 mM HEPES pH 7.5, 250 mM NaCl, 5% glycerol, 10 mM DTT with 1.0 μL of a solution containing 0.1 M BisTrisPropane pH 6.5, 0.2 M Na_2SO_4, 20% PEG 3350, 10% ethylene glycol, and 0.5% DMSO. Crystals of phosphorylated PIM-1 were grown at 4 °C in 150 nL sitting drops mixing 50 nL of PIM-1 (10 mg/mL in 50 mM HEPES pH 7.5, 280 mM NaCl, 5% glycerol,10 mM DTT) with 100 nL of a solution containing 0.1 M BisTrisPropane pH 7.5, 0.2 M Na_2SO_4, 20% PEG 3350, 10% ethylene glycol, and 0.5% DMSO.

Structure Determination. PIM-1 diffraction data (Table 1) were collected on a cryofrozen crystal (100 K) using a Rigaku

Table 1. Diffraction Data

	nonphosphorylated	phosphorylated
	Data Collection	
space group	*P*65	*P*65
cell dimensions (Å)	99.55, 99.55, 80.06	99.55, 99.55, 80.06
resolution (Å)	1.8	1.8
total observation (unique, redundancy)	289994 (41917, 6.92)	202137 (41795, 5.67)
completeness (%) (outer shell)	99.4 (98.2)	99.8 (99.7)
R_{merge} (R_{sym})	0.063 (0.781)	0.072 (0.3623)
I/σ (outer shell)	15.4 (1.5)	15.3 (3.0)
	Refinement	
R_{work} (%) (R_{free})	18.2 (21.3)	15.8 (18.3)
protein atoms (water)	2232 (242)	2257 (290)
hetero groups	sulfate, BIM-1	BIM-1
rmsd bond length (Å)	0.018	0.009
rmsd bond angle (deg)	1.914	1.602
	Ramachandran	
allowed/generally allowed/ disallowed (%)	94.1/5.9/0	94.5/5.5/0

FRE X-ray generator equipped with multilayer mirrors and an R-AXIS HTC detector. Images were indexed and integrated using MOSFLM,[26] and scaled using SCALA[27] implemented in the CCP4 (CCP4, 1994) suite of programs. Phosphorylated-PIM-1 data were collected at the PX-I beamline at the Swiss Light Source and processed with HKL2000.[28] The nonphosphorylated structure was solved using molecular replacement and the program Phaser[29] using 1MQ4 (an Aurora-related kinase) as a search model. Both structures were refined with REFMAC5[30] using iterative rounds of rigid-body refinement and restrained refinement with TLS, against maximum likelihood targets, interspersed with manual rebuilding of the model using Xfit/XtalView.[31]

Coordinates. Coordinates for the phosphorylated and unphosphorylated PIM-1 in complex with BIM-1 have been deposited in the Protein Data Bank (codes 2BIK and 1XWS, respectively). An "iSee" visualization package describing these structures and associated data and interpretation can be downloaded from our website (http://www.sgc.ox.ac.uk/structures).

Docking Procedure. The ICM docking method[32] was used for all docking experiments. This approach performs a flexible ligand/grid receptor docking process using an extended Empirical Conformation Energy Program for Peptides 3 (ECEPP/3)[33] force field and partial charges from the Merck Molecular Force Field (MMFF).[34] Potential grids are calculated (including van der Waals, electrostatic, hydrogen bond, and hydrophilic potentials), which are then applied to the molecule to be docked and the side chains of the receptor site using a global optimization method. This is based upon a series of biased-probability Monte Carlo algorithm[35] and local energy minimization steps. This approach also allows for the incorporation of energy terms that have no derivatives, such as surface-based solvation energy, using a double-energy Monte Carlo minimization method.[36] The ability for protein side chains within the receptor site to rotate helps to relieve unfavorable contacts and also promote positive interactions between the docked ligand and protein.

The docking process involves two main steps: first with only the ligand flexible and second with the ligand and receptor side chains flexible (refinement) which allows for a rapid conformational search in the first step followed by removal of unrealistic conformations before they are refined in the second step.

Results

Overall structure of PIM-1. The structure of PIM-1 in complex with the BIM-1 inhibitor was solved in both the nonphosphorylated and phosphorylated states to 1.8 Å resolution (Figure 1A). The overall structure shows the typical bilobal protein kinase architecture with the catalytic domains positioned in a constitutively closed conformation, consistent with previous PIM-1 structural studies.[16−18] The closest structural relative is the active form of the Aurora-A protein kinase (pdb entry 1OL5), which has a backbone rmsd of 3.3 Å for the full length protein and only 1.7 Å for the C-terminal kinase lobe alone. Superimposition gives Asp200 equivalence with phosphorylated Thr288 in active Aurora-A, suggesting that this residue mimics a phosphorylation site in this constitutively active kinase. Also, other conserved residues important for catalysis and cofactor binding are correctly oriented and form interactions typical for active kinases. For example, Lys67 which interacts with phosphates in ATP forms a salt bridge with Glu89 in helix αC. General structural aspects of PIM-1 kinase have been discussed previously.[16−18]

The presence of a single phosphate was evident in LC−ESI-MS. The location of the site was subsequently identified by electron density at Ser261. This modification induces no conformational change and lying at the base of the C-terminal domain has no affect on activity or inhibitor binding (data not shown). As a consensus Arg-X-X-Ser PIM-1 target sequence it could, however, have a potential role regulating PIM-1 protein interactions or stability in vivo.

The Mode of Binding of Bisindolylmaleimide I (BIM-1). The conformation of BIM-1 is very well supported by electron density (Figure 1B) showing that the PIM-1 hinge backbone interacts with the maleimide carbonyl as found for staurosporine as well as other bisindolylmaleimides.[37] However, in contrast to structures determined of PDK1−BIM complexes, the PIM-1 hinge region leaves only one hydrogen bond opportunity between the backbone carbonyl of Glu121 (equivalent to Ser160 in PDK1) and the maleimide nitrogen. Hydrogen bonding to the two additional maleimide oxygens is satisfied in PDK1 using the amide of the hinge residue Ala162 and the side chain of Thr222, while neither interaction is possible in PIM-1 which has Pro123 and Ile185 in these positions, respectively.

BIM-1 fits nicely in the hydrophobic pocket created by the glycine rich loop of PIM-1 and is enclosed by a number of other hydrophobic contacts with the residues Leu44, Val52, Ala65, Ile104, Leu120, Leu174, and Ile185 (Figure 1C). Notably, the side chain of Phe49 is positioned to form a stacking interaction with the top of the second indole ring and its hydrophobic tail, similar to the interaction seen in the PKA−BIM-2 complex.[38] This interaction is absent in PDK1 where the β-turn pulls the corresponding Phe93 out of the ATP pocket such that it makes no contact with BIM-1.

We determined a binding constant of $9.9 \pm 2.2\ 10^7$ M^{-1} (K_D 10 nM) for BIM-1 to nonphosphorylated PIM-1 using isothermal titration calorimetry (ITC). Binding is strongly driven by binding enthalpy (−14.3 kcal/mol) (Figure 3A), reflecting the favorable polar interactions attained by the rotational freedom of the two indole rings (Figure 1D). In comparison, staurosporine bound with a slightly higher affinity (K_D 1.4 nM) associated with a reduced enthalpy, but increased entropy (Table 3).

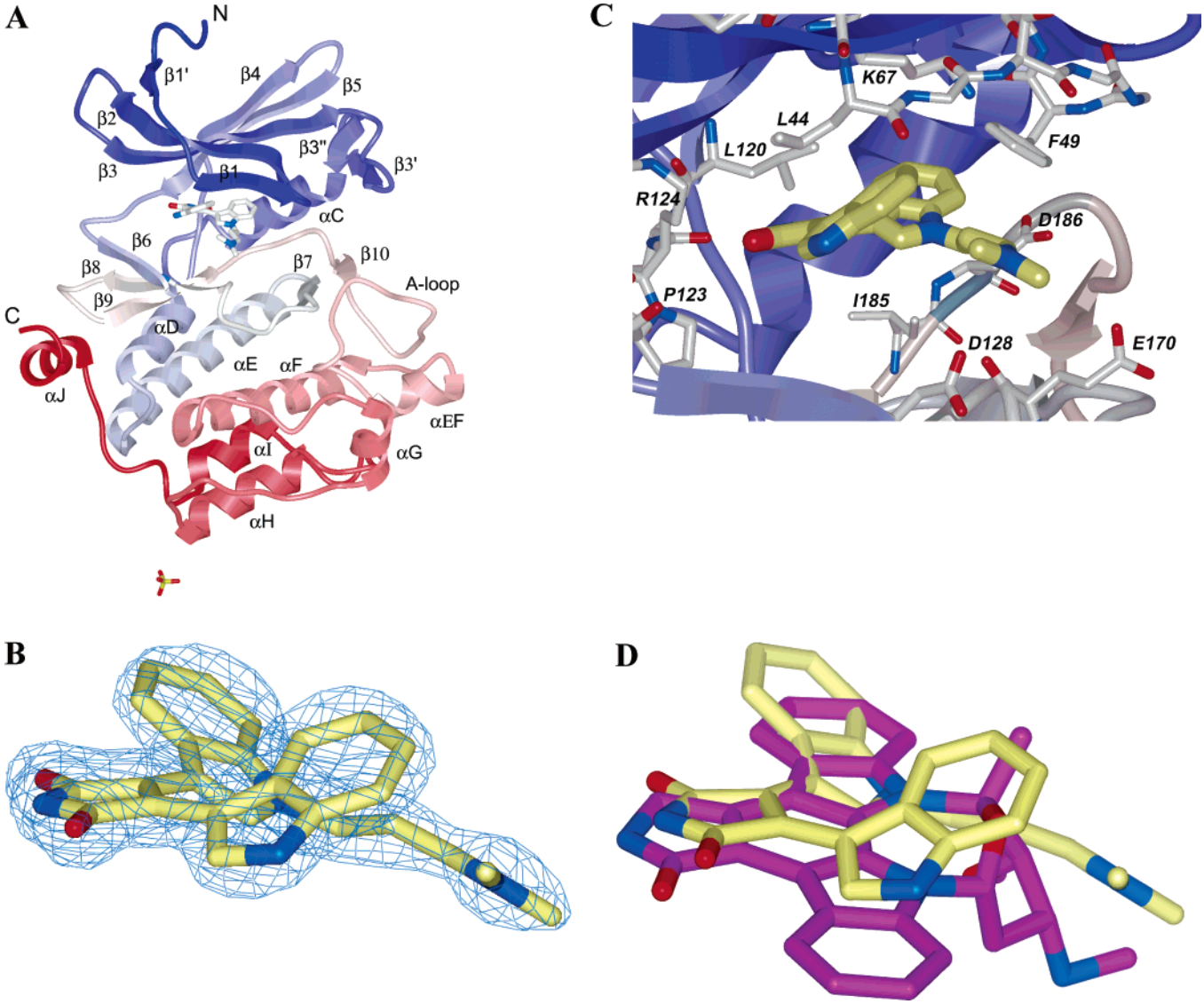

Figure 1. (A) Structural overview of PIM-1 in complex with BIM-1. The main secondary structure elements, the N- and C-termini of the protein as well as the activation loop are labeled. (B) Conformation of BIM-1 when bound to PIM-1. The electron density ($2F_oF_c$) is shown in blue. (C) Binding of BIM-1 to the hinge region of PIM-1. Residues in the vicinity of the inhibitor have been labeled. (D) Comparison of BIM-1 and staurosporine binding to the active site of PIM-1. The main chains of both structures (pdb codes 1XWS and 1YMS) have been superimposed to generate the overlay. Staurosporine carbon atoms are shown in magenta, and BIM-1 carbon atoms are shown in yellow.

PIM-1 Inhibition by Bisindolylmaleimides. The bisindolylmaleimide scaffold was screened further using compounds with four types of side groups (Figure 2: (i) hydrogen only (BIM-4); (ii) a single aliphatic side chain (BIMs 1, 8, and 9); (iii) a cyclic side chain fused to a one indole (BIMs 10 and 11); and (iv) an extended side chain tether between the two indole rings (BIM-A to E)). The original hit BIM-1 appears to belong to the subgroup with the highest PIM-1 affinity, with measured K_Ds for BIM-1, BIM-8, and BIM-9 of 8−12 nM by ITC (Table 3). This is supported by the low IC_{50} of 27 nM for BIM-1 and the effective inhibition shown by all three compounds when screened in the low micromolar range (Table 2). The loss of the aliphatic moiety in BIM-4 has only a minor effect (K_D = 27 nM), indicating that the large enthalpic contribution to binding is derived primarily from the core bisindolylmaleimide.

The additional methyl on one indole ring and the increased bulkiness of the R^1 cyclic side group in BIM-10 and BIM-11 (K_D = 72 and 250 nM, respectively) introduce steric constraints with the PIM-1 residues Val126, Asp128, and Glu171. This is shown by their significant loss in binding enthalpy, which is partly rescued by favorable entropic contribution to the binding. Accordingly, BIM-10 has an estimated IC_{50} of about 1 μM with 45% PIM-1 activity remaining at this concentration (Table 2). The BIM-11 R^1 aliphatic side chain extends by an additional methyl group and allows over 90% PIM-1 activity in the presence of this inhibitor at 1 μM.

Using this set of closely related BIM compounds we evaluated a melting temperature shift assay,[25] as a direct ligand binding assay for high throughput inhibitor screening. As a result of the law of mass action, ligand binding to the native protein is observed as a relative increase in the protein's melting temperature (T_m shift), proportional to both binding affinity and ligand concentration. The reference temperature is measured as the T_m of the ligand-free protein, which for PIM-1 was relatively low at 41 °C. In this test study

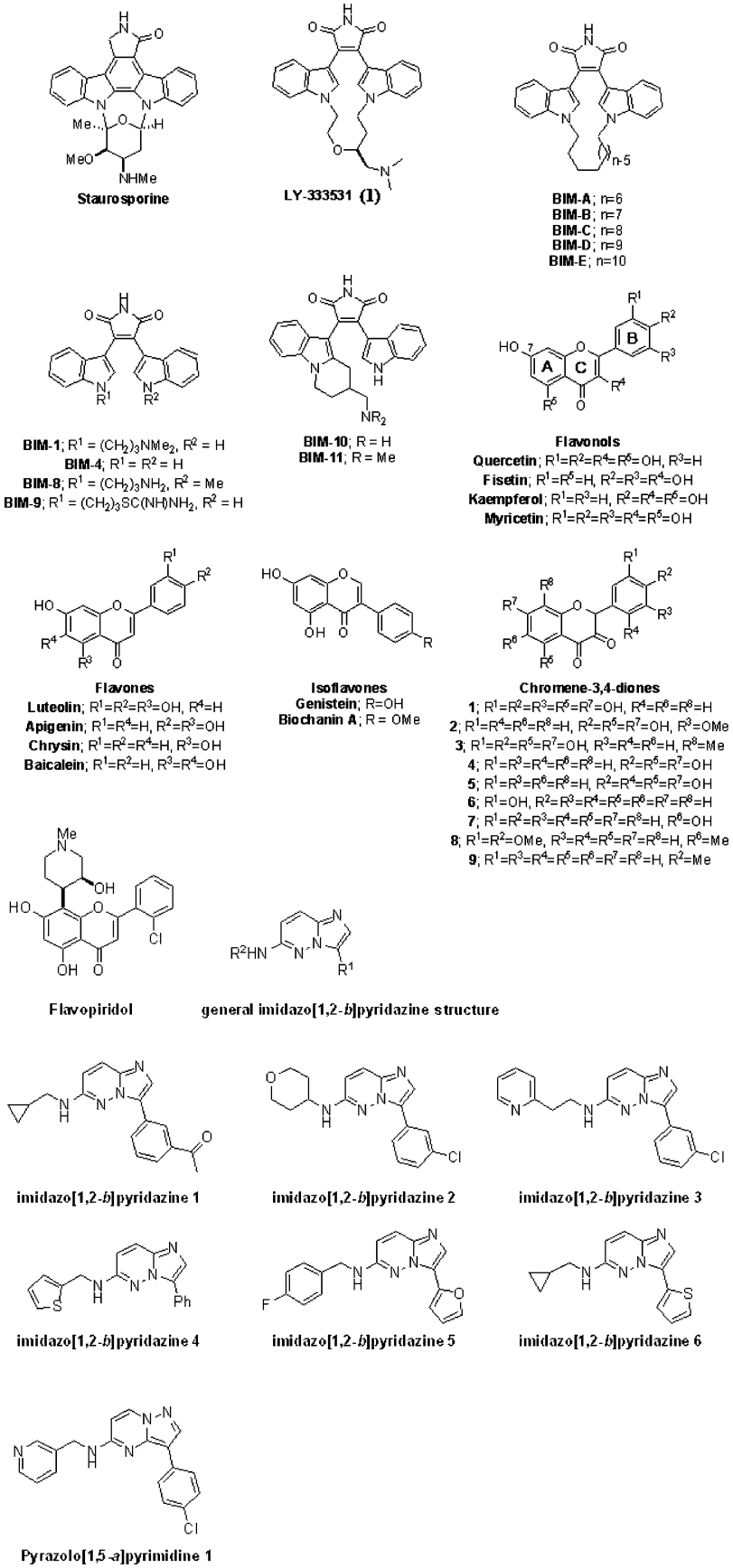

Figure 2. Inhibitor structures and assigned compound names used in this study.

we observe an excellent correlation ($R = 0.98$) between the observed T_m shifts and the K_B values determined directly by ITC (Figure 3B). Furthermore, when this approach is extended to our entire inhibitor screen, a correlation can also be seen between T_m shifts and inhibition data at 1 μM inhibitor concentration, sug-

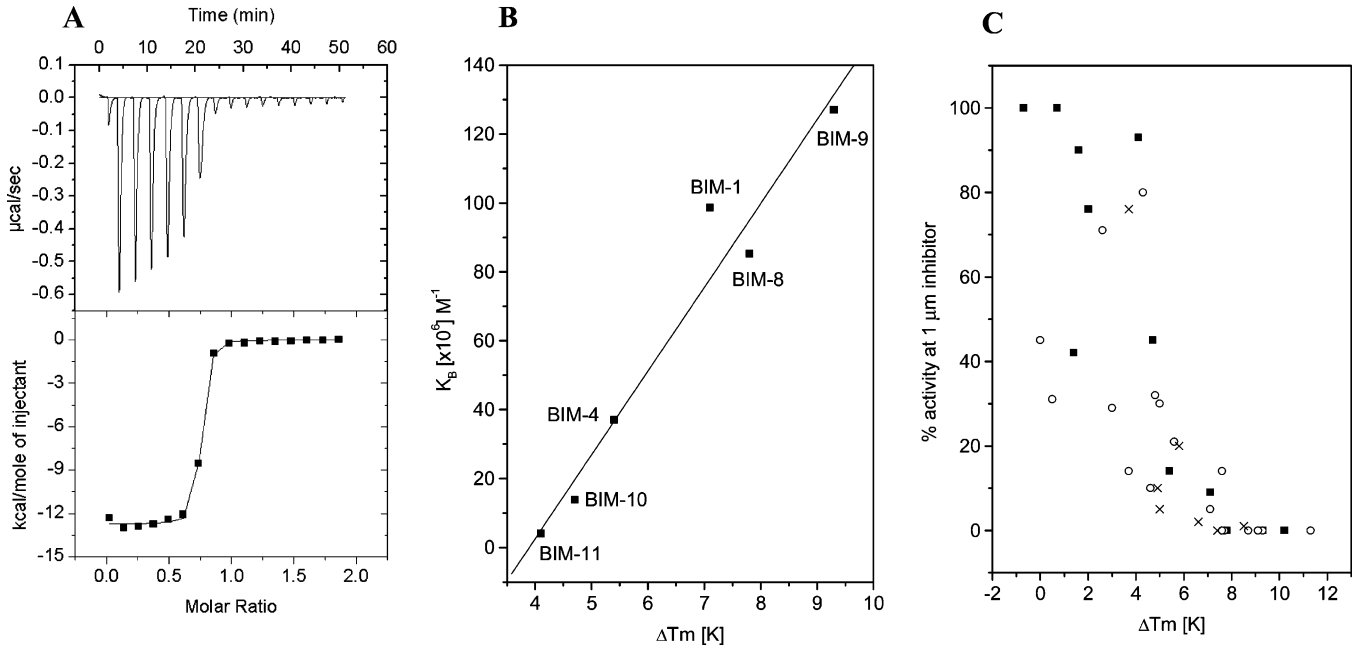

Figure 3. (A) Isothermal titration calorimetry data of BIM-1 binding to PIM-1. The protein has been titrated into a solution of the ligand in 50 mM HEPES, 150 mM NaCl, and 1 mM DTT at 10 °C. Raw binding data are shown in the upper panel of the figure. A normalized binding isotherm is shown in the lower panel. Data were fitted using a one binding site model implemented in the Origin software. The best fitting function is shown as a solid line, and fitting parameters of this experiment are summarized in Table 3. (B) Plot of melting temperature (T_m) versus the binding constants (K_B) determined by ITC. Data were fitted with a linear function ($R = 0.98$). (C) Plot of melting temperature (T_m) versus enzyme kinetic data (% inhibition at 1 μM inhibitor concentration). Bisindolylmaleimides, flavonoids, and imidazopyridazines are shown by solid black squares, open circles, and crosses, respectively.

gesting that this assay is a general method for the identification of both weak (low micromolar) and strongly interacting ligands (Figure 3C).

The subset of tethered bisindolylmaleimide compounds, BIM-A to E, lie at the detection limit of this analysis, producing no significant T_m shift in screening. However, BIM-E showed a second melting transition consistent with a stabilizing ligand interaction (Table 2). Indeed, there seems to be a noteworthy correlation between binding and the length of the macrocyclic tether with BIM-A and BIM-E giving 0 and 100% inhibition, respectively, at 10 μM concentration. Previous work suggests that the shorter tether prevents the idealized (i.e. tether-free) geometry of the two indole rings; thus the right tether length might constrain the two indole rings in a conformation similar to this ideal and significantly reduce any unfavorable entropic contributions to binding.

1, a related bisindolylmaleimide derivative with a heterocyclic tether, is also reported to bind tightly to PIM-1 with a K_D of 55 nM.[39] We used the BIM-1 complex as a model for the docking of this compound. The best docking model reproduced the binding mode observed in the PDK1 complex[37] (Figure 4A). In order to accommodate this inhibitor the glycine rich loop residue Phe49 needs to flip out of the ATP pocket to assume a conformation similar to that observed in the AMP−PNP complex.[16]

PIM-1 Inhibition by Flavonoids. The flavonoid inhibitors were found to have comparable potential against PIM-1 as the bisindolylmaleimides. To investigate their structure−activity relationships, screens were undertaken against four flavonoid scaffolds: (i) flavonols, (ii) flavanones, (iii) flavones, and (iv) isoflavones (Figure 2). The span of their affinities is several orders of magnitude greater than the bisindolylmaleimides studied by ITC. Also here a good correlation is observed between our coarse ligand screen using T_m shift values and kinase inhibition data (Figure 3C). These combined data show PIM-1 to bind with highest affinity first to flavonols > flavones > isoflavones while the flavanone derivatives used in this study vary across this range depending on the various R groups present (Table 2). These results are consistent with the known specificity of isoflavones such as genistein for the tyrosine protein kinase family compared to their inactivity against serine-threonine protein kinases such as PIM-1.[47]

Flavonols and Flavanones. The two most potent inhibitors of the flavonoid class identified in this study were quercetin and fisetin. Quercetin bound with a K_D of 25 nM as determined by ITC and had an IC_{50} of 43 nM in enzyme kinetic assays. In fact all four flavonols tested showed comparable inhibitory activity within the experimental error, giving complete inhibition at 1 μM concentration. Kaempferol differs from myricetin by the absence of R^1 and R^3 hydroxyls, suggesting that a single hydrogen bond donor on ring B is sufficient. The flavanones tested in this study are a series of chromene-3,4-dione derivatives that substitute the R^4 flavonol hydroxyl with a keto group conserving the potential hydrogen bond with the hinge anchor residue, Glu121. Apart from this, the flavanone chromene-3,4-dione 1 is similar to myricetin and shows a comparable T_m shift and enzymatic inhibition (Table 2). Similar results for chromene-3,4-dione 2 show that substitution of OCH_3 for OH at R^3 is well tolerated (for example, ring B is free to rotate out of plane with the double ring system). However, the introduction of a methyl group at R^8 in

Table 2. Screen of Potential PIM-1 Inhibitors

inhibitor	ΔT_m^{obs} [a] (°C)	% activity[c] 1 μM inhibitor	% activity[c] 10 μM inhibitor
staurosporine	10.2 ± 0.3 (3)	0 ± 0 (3)	0 ± 0 (3)
bisindolylmaleimides			
BIM-1	7.1 ± 0.2 (3)	9 ± 2 (3)	5 ± 1 (3)
BIM-4	5.4 ± 0.4 (3)	14 ± 3 (3)	8 ± 1 (3)
BIM-8	7.8 ± 0.3 (3)	0 ± 0 (3)	0 ± 0 (3)
BIM-9	9.3 ± 0.4 (3)	0 ± 0 (3)	0 ± 0 (3)
BIM-10	4.7 ± 0.2 (3)	45 ± 6 (3)	13 ± 3 (3)
BIM-11	4.1 ± 0.4 (3)	93 ± 3 (3)	34 ± 6 (3)
BIM-A	−0.7 (1)	100 (1)	100 ± 0 (2)
BIM-B	0.7 ± 1.2 (2)	100 (1)	80 ± 3 (2)
BIM-C	2.0 (1)	76 (1)	30 ± 6 (2)
BIM-D	1.6 ± 0.5 (2)	90 (1)	76 ± 3 (2)
BIM-E	1.4 ± 0.4 (2)[b]	42 ± 6 (2)	0 ± 0 (2)
flavonoids			
quercetin	11.3 ± 0.3 (4)	0 ± 0 (3)	0 (1)
fisetin	9.3 ± 0.6 (3)	0 ± 0 (2)	0 (1)
kaempferol	9.1 ± 0.5 (3)	0 (1)	0 (1)
myricetin	8.7 ± 0.4 (3)	0 (1)	0 (1)
luteolin	7.6 ± 0.7 (3)	14 ± 3 (2)	0 (1)
apigenin	5.6 ± 0.2 (3)	21 (1)	16 (1)
chrysin	4.8 ± 0.3 (3)	32 (1)	16 (1)
baicalein	3.0 ± 1.2 (3)	29 (1)	17 (1)
genistein	2.6 ± 0.6 (3)	71 (1)	65 (1)
biochanin A	4.3 ± 0.6 (3)	80 (1)	69 (1)
chromene-3,4-dione 1	7.7 ± 0.9 (3)	0 ± 0 (2)	0 ± 0 (2)
chromene-3,4-dione 2	9.1 ± 0.7 (3)	0 (1)	0 (1)
chromene-3,4-dione 3	5.0 ± 0.7 (3)	30 (1)	7 (1)
chromene-3,4-dione 4	7.1 ± 0.8 (3)	5 (1)	0 (1)
chromene-3,4-dione 5	7.6 ± 0.5 (4)	0 (1)	0 (1)
chromene-3,4-dione 6	4.6 ± 0.3 (3)	10 (1)	0 (1)
chromene-3,4-dione 7	3.7 ± 0.4 (3)	14 (1)	0 (1)
chromene-3,4-dione 8	0.0 ± 0.1 (3)	45 (1)	28 (1)
chromene-3,4-dione 9	0.5 ± 0.1 (3)	31 (1)	22 (1)
imidazopyridazine			
imidazo[1,2-*b*]pyridazine 1	6.6 ± 0.3 (3)	2 ± 1 (2)	0 (1)
imidazo[1,2-*b*]pyridazine 2	8.5 ± 0.3 (3)	1 (1)	0 (1)
imidazo[1,2-*b*]pyridazine 3	7.4 ± 0.1 (3)	0 (1)	0 (1)
imidazo[1,2-*b*]pyridazine 4	3.7 ± 0.2 (3)	76 (1)	15 (1)
imidazo[1,2-*b*]pyridazine 5	5.0 ± 0.8 (3)	5 (1)	0 (1)
imidazo[1,2-*b*]pyridazine 6	5.8 ± 0.3 (3)	20 (1)	2 (1)
pyrazolo[1,5-*a*]pyrimidine 1	4.9 ± 0.2 (3)	10 (1)	5 (1)

[a] Apparent T_m shift upon inhibitor binding ± standard error. Number of repeats in parentheses. 10 μM inhibitor. [b] BIM-E at 20 μM showed two transitions upon denaturation: 3.5 °C and a less populated transition at 11.4 °C. [c] Activity as a percentage of the maximum rate observed in the absence of inhibitor ± standard error. Number of repeats in parentheses.

Table 3. ITC and Binding Data for Selected PIM-1 Inhibitors and Determined IC_{50} Values

inhibitor	ΔT_m^{obs} [a] (°C)	IC_{50} (nM)	K_D (nM)	$K_B \times 10^6$ (M^{-1})	ΔH^{obs} (kcal/mol)	$T\Delta S$ (kcal/mol)	ΔG (kcal/mol)	N[b]
quercetin	11.3	43	25	39.3 ± 6.3	−9.6 ± 0.1	0.26	−9.8	0.97
staurosporine	10.2		1.4	705 ± 345	−8.1 ± 0.1	3.34	−11.5	0.85
BIM-1	7.1	27	10	98.6 ± 21.7	−14.3 ± 0.1	−3.85	−10.4	0.64
BIM-4	5.4		27	37.0 ± 4.0	−10.4 ± 0.1	−0.55	−9.8	0.45
BIM-8	7.8		12	85.2 ± 15.5	−9.9 ± 0.1	0.39	−10.3	0.57
BIM-9	9.3		8	127 ± 36	−10.7 ± 0.1	−0.22	−10.5	0.61
BIM-10	4.7		72	13.8 ± 3.0	−5.6 ± 0.1	3.59	−9.2	0.88
BIM-11	4.1		250	4.0 ± 1.3	−3.3 ± 0.1	5.29	−8.5	0.58
imidazo[1,2-*b*]pyridazine 1	6.6	61	25	39.7 ± 13.6	−5.2 ± 0.1	4.67	−9.8	0.57
staurosporine		10[d]	15[c]					
BIM-1		150[d]						
BIM-9		10[d]						
flavopiridol			520[c]					
LY-333531			55[c]					

[a] Average value from Table 2. [b] Stoichiometry determined from a single binding site model. [c] Published PIM1-T7 phage fusion affinity data.[39] [d] Published.[17]

chromene-3,4-dione 3 decreases the T_m by 5 °C and raises the PIM-1 activity at 1 μM inhibitor concentration to 30%. Chromene-3,4-diones 8 and 9 were the least potent inhibitors detected in this study and lack hydroxyl groups anywhere within their structure.

Flavones and Isoflavones. In contrast to the flavonols and several flavanones, the four flavones tested all fail to show complete inhibition at 1 μM concentration. Luteolin and apigenin differ from quercetin and kaempferol, respectively, by the single absence of the

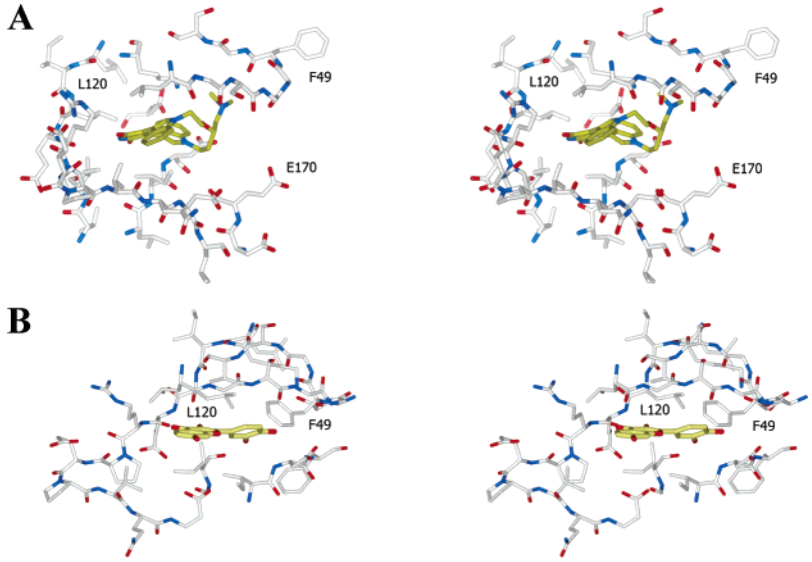

Figure 4. (A) Docking model of **1** into the ATP binding site of PIM-1. The determined binding mode represented the model with lowest pseudo-energy term and reproduced well the binding mode observed for this compound in complex with PDK1.[37] Inhibitor carbon atoms are shown in yellow. For reasons of clarity only some residues have been labeled. (B) Docking model of the flavonoid fisetin. Atoms are colored as shown as in Figure 4A.

R^4 hydroxyl showing the importance of this side group. Chrysin and baicalein also lack any hydroxyl substituent on ring B. Notably, baicalein produces a T_m shift (3 °C) less than half that of the best flavone, luteolin (7.6 °C). However, the comparable inhibition profiles of apigenin, chrysin, and baicalein suggest that chrysin and baicalein may bind in an alternative orientation to restore some hydrogen bonding potential. Both isoflavones tested show less than 50% inhibition of PIM-1 activity even at the higher inhibitor concentration of 10 μM.

The Mode of Binding of Flavonoids from PIM-1 Docking Studies. From the known structures of CDK2−deschloroflavopiridol,[40] CDK6−fisetin,[41] and Hck−quercetin,[42] flavonoids are expected to anchor to the kinase hinge region competing for the same hydrogen bonds as the N1 and N6 nitrogens of ATP. Despite the occurrence of Pro123 at the third hinge residue, the docking model of the PIM-1−fisetin complex (Figure 4B) reproduced the binding orientation observed in the corresponding CDK6−fisetin structure and was comparable to a simple superimposition of the two structures. The PIM-1 proline substitution removes the amide hydrogen bond donor to the carbonyl oxygen of ring C, but the first hinge residue, Glu121, provides a backbone hydrogen bond acceptor for the R^4 hydroxyl. This binding mode places ring B deep into the ATP pocket where the R^2 and R^3 hydroxyls form a strong hydrogen bonding network with the catalytic residues Lys67, Glu89, and Asp186, which are also conserved in CDK6. Similarly, PIM-1 satisfies a conserved hydrogen bond between the C-7 hydroxyl (ring A) and Asp128.

In the CDK2−deschloroflavopiridol[43] and Hck−quercetin[44] complexes the additional R^5 hydroxyl replaces the fisetin R^4-hinge interaction through a ligand rotation of ~180° around the hydrogen bond between the third hinge residue and the ring C carbonyl. This anchor point is unavailable in PIM-1, and docking of the quercetin complex was inconclusive. In either ligand orientation the R^2 side group would be positioned to form a direct hydrogen bond with either Glu89 or Asp131. In the absence of R^2 or other ring B hydroxyl groups, the docked PIM-1−chrysin complex suggested an interaction between R^3 and Asp186 and between the C-7 hydroxyl and Asp128/Glu171 (not shown).

Imidazo[1,2-*b*]pyridazines and Pyrazolo[1,5-*a*]-pyrimidines. We also established a SAR of novel kinase inhibitor scaffolds as PIM-1 inhibitors. This included a small kinase-targeted compound collection obtained from BioFocus (Cambridge, U.K.) biased toward simple scaffolds that are prospective low affinity compounds for lead development. Ten compounds from a 96-well plate of this collection produced a significant T_m shift (>2 °C) which belonged to two similar scaffolds: imidazo[1,2-*b*]pyridazines and pyrazolo[1,5-*a*]-pyrimidines. Compounds with the largest T_m shift were effective PIM-1 inhibitors at 1 μM (Table 2). Indeed, the compound imidazo[1,2-*b*]pyridazine 1 had an IC_{50} of 61 nM and a dissociation constant measured by ITC of 25 nM (Table 3). Even with this remarkably high affinity there appears to be opportunity for further optimization as the majority of compounds tested from these two scaffolds were classed as significant hits (T_m shift >2 °C). The ITC data show highly favorable binding entropy but a moderate enthalpy, suggesting that polar interaction of this inhibitor class with PIM-1 should be improved.

It is noteworthy that the positions of the R^1 and R^2 groups are conserved across both scaffolds and in the weakest hit, imidazo[1,2-*b*]pyridazine 4, these substitutions are purely hydrophobic (Figure 2). Variation of these two scaffolds to alter the R^1 and R^2 positions appears unfavorable (Figure 5). For example 34 compounds with the imidazo[1,2-*a*]pyrazine scaffold were tested including such alterations but failed to produce a significant T_m shift. The compound library consisted largely of disubstituted compounds, and one substitution at the C-7 position of the successful imidazo[1,2-*b*]-pyridazine scaffold remains to be explored. Attempts to dock either scaffold into the PIM-1 ATP binding pocket failed to identify a single low-energy binding mode.

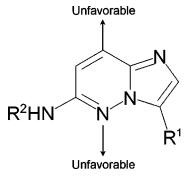

Figure 5. SAR conclusions for imidazopyridazine and pyrazolopyrimidine-type inhibitors of PIM-1 (imidazo[1,2-*b*]pyridazine scaffold shown). Compounds showing a significant T_m shift (>2 °C) were imidazo[1,2-*b*]pyridazin-6-amines and pyrazolo[1,5-*a*]pyrimidin-5-amines, both with at least a monocyclic aromatic C-3 substitution (R^1). Ring positions with substitutions providing no significant T_m shift are labeled unfavorable. These compounds included C-3 and C-5 substituted imidazo-[1,2-*a*]pyrazin-8-amines. Other ring positions were not investigated in detail.

Conclusions

A large body of biological data suggests inhibition of PIM-1 as an interesting point of intervention to treat certain human leukemia and lymphomas. Due to the unique hinge region (characterized both by an atypical conformation and by the lack of a hydrogen bond donor at position 123) it is of particular importance to examine how PIM-1 binds small molecule inhibitors. The lack of this hydrogen bond donor in kinases of the PIM family has been reported to produce a significantly altered selectivity toward small molecules as compared to other serine/threonine protein kinases. For example, in a recent publication by Kumar et al. an unexpected binding mode for AMP and an inhibitor of the oxindole class have been described.[18] However, the high-resolution structure of PIM-1 in complex with BIM-1 revealed no unexpected differences in binding mode when compared with cocrystal structures of this compound with the kinase PDK1.[37] Also a subsequent screening of a kinase targeted library identified several typical ATP mimetic kinase inhibitors as high affinity ligands of PIM-1 suggesting that the missing hydrogen bond in the hinge region can be well tolerated. However, the lack of a second hydrogen bond donor made docking of compounds into the active site of PIM-1 a difficult task and we presented here only models that resulted in a unique low energy conformation which was well supported by the established SAR.

In addition to traditional methods such as activity assays and isothermal titration calorimetry (ITC), we employed a facile T_m shift assay to rapidly screen for putative PIM-1 inhibitors. Ligand binding is simply detected as a relative increase in the protein's melting temperature, proportional to ligand concentration and affinity. This methodology was found to be very robust and reliable, and the data correlate well with both activity and calorimetrically determined binding constants. A linear relationship was found for the determined binding constant and the shift in melting temperature suggesting that once the data have been calibrated for a certain scaffold-protein system the determined temperature shift could be used to establish a SAR of the selected inhibitor class. However, it would be interesting to verify the general applicability of this methodology on a larger set of different enzymes and inhibitor systems. In principle, T_m shifts are expected to detect all binders including those that bind to cavities other than the active site, although the majority of inhibitors in our screening were well studied ATP mimetic inhibitors.

The binding of bisindolylmaleimides in this study was characterized thermodynamically by a large favorable binding enthalpy indicating favorable polar interactions. This result is quite surprising considering that one main chain and another side chain hydrogen bond cannot be formed. However, the introduced flexibility of the two indole rings has a high entropic penalty when compared with the binding of staurosporine. A possible solution to this problem is the generation of macrocyclic bisindolylmaleimides in which the indole nitrogens are linked with a tether that constrains the indole ring conformation. Thus, if the correct conformation necessary for binding is determined by the tether in solution, binding entropy changes would be expected to be more favorable when compared to the unconstrained compound. Unfortunately, the small series of this inhibitor class used in this study were either completely inactive or had rather weak inhibitory activity. In contrast, the macrocyclic bis-indolylmaleimide 1 has been reported to be a potent PIM-1 inhibitor[39] ($K_D \sim 50$ nM). Since this inhibitor has advanced to phase III human clinical trials, it might be an interesting drug candidate for treatment of human cancer. A recent publication suggests that PIM kinase inhibitors would be particularly beneficial for rapamycin-insensitive forms of leukemia and lymphoma.[45]

Several flavonoids were detected to be highly potent PIM-1 inhibitors. This compound class has been described to inhibit a large number of kinases as well as other enzymes.[46] For example, the isoflavone genistein inhibits EGFR in the submicromolar range.[47] The protection against some forms of cancer provided by many common foods has been observed in multiple epidemiological studies. Thus, flavonoids such as the synthetic flavone, flavopiridol; the soy isoflavone, genistein; the tea catechin epigallocatechin gallate; or the common dietary flavonol, quercetin, are emerging as prospective anticancer drug candidates, and some of them have already entered into clinical trials. Besides their therapeutic potential, since lots of flavonoids are present in our diet, a greater understanding of their anticancer properties might help to prevent cancer by suggesting modifications in dietary habits.[48]

SAR analysis showed a strong dependence on the availability of the flavonol R^2 and R^4 hydroxyls. The docked PIM-1−fisetin complex maintains the binding mode observed in the CDK6−fisetin crystal structure.[49] The lost hinge interaction from Pro123 appears to be compensated by a hydrogen bonding network created by the insertion of ring B deep into the ATP-binding pocket (Figure 4B). This favorable interaction site is also observed in the recent crystal structures of PIM-1 in complex with LY294002 (2-(4-morpholinyl)-8-phenyl-4*H*-l-benzopyran-4-one)[17] and the quinolinone derivative PLX-K063 (3,4-dihydroxy-1-methyl-quinolin-2-one),[18] which both utilize two conserved water molecules to achieve optimal hydrogen bonding.

Finally, PIM-1 is identified to have marked specificity for a subset of 3,6-disubstituted imidazo[1,2-*b*]pyridazine and 3,5-disubstituted pyrazolo[1,5-*a*]pyrimidine scaffolds which represent novel derivatives of these inhibitor classes. SAR analysis shows a requirement for

these equivalent ring substitutions and intolerance for other disubstituted alternatives (Figure 5). Pyrazolopyrimidine-type inhibitors were first described as specific inhibitors of the Src-family of tyrosine kinases with several pyrazolo[3,4-*d*]pyrimidines having low nanomolar affinity for Lck and anticancer activity.[50] One of these compounds, PP1, was later crystallized in complex with the autoinhibited form of Hck, providing further guidance for drug development.[51] Subsequently this scaffold has yielded specific inhibitors for glycogen synthase kinase-3 (GSK-3)[52] and members of the CDK family.[53,54] Inhibitors based on the variant pyrazolo[1,5-*a*]pyrimidine scaffold have also been described with specificity for CDK2[55] and the KDR kinase domain.[56] Additionally, CDK2 has been cocrystallized with both imidazo[1,2-*a*]pyridine[57,58] and imidazo[1,2-*b*]pyridazine compounds.[59] Unfortunately, attempts to cocrystallize or conclusively dock these inhibitors with PIM-1 were unsuccessful. However, the potential diversity of substituent groups and their ring positions appears to provide great opportunity for further diversification of these scaffolds, and PIM-1 appears to have novel specificity in this regard. Here we identify a lead candidate of the imidazo[1,2-*b*]pyridazine class with an affinity for PIM-1 of 25 nM. Originating from a screen of about 100 novel compounds, further development of this scaffold might lead to interesting clinical candidates for the treatment of human cancer.

Acknowledgment. We thank Dr. Kunde Guo for cloning and expression testing of PIM-1 constructs, Dr. Frank von Delft for diffraction data collection, Dr. Wen Hwa Lee for help with the ICM-Pro visualization software, and Dr. Michael Sundstrum and Dr. Susanne Muller-Knapp for critical reading of the manuscript. The Structural Genomics Consortium is a registered charity (No. 1097737) funded by the Wellcome Trust, GlaxoSmithKline, Genome Canada, the Canadian Institutes of Health Research, the Ontario Innovation Trust, the Ontario Research and Development Challenge Fund, and the Canadian Foundation for Innovation.

References

(1) Cuypers, H. T. Virus integration. *Cell* **1984**, *37*, 141−150.
(2) Mikkers, H.; Nawijn, M.; Allen, J.; Brouwers, C.; Verhoeven, E.; Jonkers, J.; Berns, A. Mice deficient for all PIM kinases display reduced body size and impaired responses to hematopoietic growth factors. *Mol. Cell. Biol*. **2004**, *24*, 6104−6115.
(3) Bachmann, M.; Möröy, T. The serine/threonine kinase Pim-1. *Int. J. Biochem. Cell Biol*. **2005**, *37*, 726−730.
(4) Shirogane, T.; Fukada, T.; Muller, J. M.; Shima, D. T.; Hibi, M.; Hirano, T. Synergistic roles for Pim-1 and c-Myc in STAT3-mediated cell cycle progression and antiapoptosis. *Immunity* **1999**, *11*, 709−719.
(5) Wang, Z.; Bhattacharya, N.; Weaver, M.; Petersen, K.; Meyer, M.; Gapter, L.; Magnuson, N. S. Pim-1: a serine/threonine kinase with a role in cell survival, proliferation, differentiation and tumorigenesis. *J. Vet. Sci*. **2001**, *2*, 167−179.
(6) Chen, X. P.; Losman, J. A.; Cowan, S.; Donahue, E.; Fay, S.; Vuong, B. Q.; Nawijn, M. C.; Capece, D.; Cohan, V. L.; Rothman, P. Pim serine/threonine kinases regulate the stability of Socs-1 protein. *Proc. Natl. Acad. Sci. U.S.A*. **2002**, *99*, 2175−2180.
(7) Peltola, K. J.; Paukku, K.; Aho, T. L.; Ruuska, M.; Silvennoinen, O.; Koskinen, P. J. Pim-1 kinase inhibits STAT5-dependent transcription via its interactions with SOCS1 and SOCS3. *Blood* **2004**, *103*, 3744−3750.
(8) van Lohuizen, M.; Verbeek, S.; Krimpenfort, P.; Domen, J.; Saris, C.; Radaszkiewicz, T.; Berns, A. Predisposition to lymphomagenesis in pim-1 transgenic mice: cooperation with c-myc and N-myc in murine leukemia virus-induced tumors. *Cell* **1989**, *56*, 673−682.
(9) Roh, M.; Gary, B.; Song, C.; Said-Al-Naief, N.; Tousson, A.; Kraft, A.; Eltoum, I. E.; Abdulkadir, S. A. Overexpression of the oncogenic kinase Pim-1 leads to genomic instability. *Cancer Res*. **2003**, *63*, 8079−8084.
(10) Valdman, A.; Fang, X.; Pang, S. T.; Ekman, P.; Egevad, L. Pim-1 expression in prostatic intraepithelial neoplasia and human prostate cancer. *Prostate* **2004**, *60*, 367−371.
(11) Pircher, T. J.; Zhao, S.; Geiger, J. N.; Joneja, B.; Wojchowski, D. M. Pim-1 kinase protects hematopoietic FDC cells from genotoxin-induced death. *Oncogene* **2000**, *19*, 3684−3692.
(12) Akasaka, H.; Akasaka, T.; Kurata, M.; Ueda, C.; Shimizu, A.; Uchiyama, T.; Ohno, H. Molecular anatomy of BCL6 translocations revealed by long-distance polymerase chain reaction-based assays. *Cancer Res*. **2000**, *60*, 2335−2341.
(13) Pasqualucci, L.; Neumeister, P.; Goossens, T.; Nanjangud, G.; Chaganti, R. S.; Kuppers, R.; Dalla-Favera, R. Hypermutation of multiple protooncogenes in B-cell diffuse large-cell lymphomas. *Nature* **2001**, *412*, 341−346.
(14) Montesinos-Rongen, M.; Van Roost, D.; Schaller, C.; Wiestler, O. D.; Deckert, M. Primary diffuse large B-cell lymphomas of the central nervous system are targeted by aberrant somatic hypermutation. *Blood* **2004**, *103*, 1869−1875.
(15) Gaidano, G.; et al. Aberrant somatic hypermutation in multiple subtypes of AIDS-associated non-Hodgkin lymphoma. *Blood* **2003**, *102*, 1833−1841.
(16) Qian, K. C.; Wang, L.; Hickey, E. R.; Studts, J.; Barringer, K.; Peng, C.; Kronkaitis, A.; Li, J.; White, A.; Mische, S.; Farmer, B. Structural basis of constitutive activity and a unique nucleotide binding mode of human Pim-1 kinase. *J. Biol. Chem*. **2005**, *280*, 6130−6137.
(17) Jacobs, M. D.; Black, J.; Futer, O.; Swenson, L.; Hare, B.; Fleming, M.; Saxena, K. PIM-1 ligand bound structures reveal the mechanism of serine/threonine kinase inhibition by LY294002. *J. Biol. Chem*. **2005**, *280*, 13728−12734.
(18) Kumar, A.; Mandiyan, V.; Suzuki, Y.; Zhang, C.; Rice, J.; Tsai, J.; Artis, D. R.; Ibrahim, P.; Bremer, R. Crystal structures of proto-oncogene kinase Pim1: a target of aberrant somatic hypermutations in diffuse large cell lymphoma. *J. Mol. Biol*. **2005**, *348*, 183−193.
(19) Goekjian, P. G.; Jirousek, M. R. Protein kinase C in the treatment of disease: signal transduction pathways, inhibitors, and agents in development. *Curr. Med. Chem*. **1999**, *6*, 877−903.
(20) Davies, S. P.; Reddy, H.; Caivano, M.; Cohen, P. Specificity and mechanism of action of some commonly used protein kinase inhibitors. *Biochem. J*. **2000**, *351*, 95−105.
(21) Davis, P. D.; Hill, C. H.; Lawton, G.; Nixon, J. S.; Wilkinson, S. E.; Hurst, S. A,; Keech, E.; Turner, S. E. Inhibitors of Protein Kinase C (1): 2,3-Bisarylmaleimides. *J. Med. Chem*. **1992**, *35*, 177−184.
(22) Duby, J. J.; Campbell, R. K.; Setter, S. M.; White, J. R.; Rasmussen, K. A. Diabetic neuropathy: an intensive review. *Am. J. Health-Syst. Pharm*. **2004**, *61*, 160−173.
(23) Bartlett, S.; Nelson, A. Evaluation of alternative approaches for the synthesis of macrocyclic bisindolylmaleimides. *Org. Biomol. Chem*. **2004**, *2*, 2874−2883.
(24) Cook, F. N.; Neville, M. E.; Vrana, K. E.; Hartl, F. T.; Roskowski, R. Adenosine cyclic 30,50-monophosphate dependent protein kinase: kinetic mechanism for the bovine skeletal muscle catalytic subunit. *Biochemistry* **1982**, *21*, 5794−5799.
(25) Matulis, D.; Kranz, J. K.; Salemme, R.; Todd, M. J. Thermodynamic stability of Carbonic Anhydrase: Measurements of binding affinity and stoichiometry using ThermoFluor. *Biochemistry* **2005**, *44*, 5258−5266.
(26) Leslie, A. G. W. *Jt. CCP4 ESF-EAMCB Newsl. Protein Crystallogr*. **1992**, 26.
(27) Evans, P. R. Data reduction. *Proc. CCP4 Study Weekend Data Collect. Process*. **1993**, 114−122.
(28) Otwinowski, Z.; Minor, W. Processing of X-ray diffraction data collected in oscillation mode. *Methods Enzymol*. **1997**, *276*, 307−326.
(29) Storoni, L. C.; McCoy, A. J.; Read, R. J. Likelihood-enhanced fast rotation functions. *Acta Crystallogr., Sect. D: Biol. Crystallogr*. **2004**, *60*, 432−438.
(30) Murshudov, G. N.; Vagin, A. A.; Dodson, E. J. Refinement of macromolecular structures by the maximum-likelihood method. *Acta Crystallogr., Sect. D: Biol. Crystallogr*. **1997**, *53*, 240−255.
(31) McRee, D. E. XtalView/Xfit−a versatile program for manipulating atomic coordinates and electron density. *J. Struct. Biol*. **1999**, *125*, 156−165.
(32) Totrov, M.; Abagyan, R. Flexible protein-ligand docking by global energy optimization in internal coordinates. *Proteins* **1997**, Suppl. 1, 215−220.
(33) Nemethy, G.,; et al. Energy parameters in polypeptides: Ten improved geometrical parameters and nonbonded interactions for use in the ECEPP/3 algorithm, with application to proline-containing peptides. *J. Phys. Chem*. **1992**, *96*, 6472−6484.

(34) Halgren, T. Merck molecular force field I-V. *J. Comput. Chem*. **1995**, *17*, 490−641.
(35) Abagyan, R.; Totrov, M. Biased probability Monte Carlo conformational searches and electrostatic calculations for peptides and proteins. *J. Mol. Biol*. **1994**, *235*, 983−1002.
(36) Abagyan, R. et al. ICM—a new method for protein modeling and design: Applications to docking and structure prediction from the native conformation. *J. Comput. Chem*. **1994**, *15*, 488−506.
(37) Komander, D.; Kular, G. S.; Schuttelkopf, A. W.; Deak, M.; Prakash, K. R.; Bain, J.; Elliott, M.; Garrido-Franco, M.; Kozikowski, A. P.; Alessi, D. R.; van Aalten, D. M. Interactions of LY333531 and other bisindolyl maleimide inhibitors with PDK1, *Structure* **2004**, *12*, 215−226.
(38) Gassel, M.; Breitenlechner, C. B.; Konig, N.; Huber, R.; Engh, R. A.; Bossemeyer, D. The protein kinase C inhibitor bisindolyl maleimide 2 binds with reversed orientations to different conformations of protein kinase A. *J. Biol. Chem*. **2004**, *279*, 23679−23690.
(39) Fabian, M. A.; et al. A small molecule-kinase interaction map for clinical kinase inhibitors. *Nat. Biotechnol*. **2005**, *23*, 329−336.
(40) De Azevedo, W. F., Jr.; Mueller-Dieckmann, H. J.; Schulze-Gahmen, U.; Worland, P. J.; Sausville, E.; Kim, S. H. Structural basis for specificity and potency of a flavonoid inhibitor of human CDK2, a cell cycle kinase. *Proc. Natl. Acad. Sci. U.S.A*. **1996**, *93*, 2735−2740.
(41) Lu, H.; Chang, D. J.; Baratte, B.; Meijer, L.; Schulze-Gahmen, U. Crystal structure of a human cyclin-dependent kinase 6 complex with a flavonol inhibitor, fisetin. *J. Med. Chem*. **2005**, *48*, 737−743.
(42) Sicheri, F.; Moarefi, I.; Kuriyan, J. Crystal structure of the Src family tyrosine kinase Hck. *Nature* **1997**, *385*, 602−609.
(43) De Azevedo, W. F., Jr.; Mueller-Dieckmann, H. J.; Schulze-Gahmen, U.; Worland, P. J.; Sausville, E.; Kim, S. H. Structural basis for specificity and potency of a flavonoid inhibitor of human CDK2, a cell cycle kinase. *Proc. Natl. Acad. Sci. U.S.A*. **1996**, *93*, 2735−2740.
(44) Sicheri, F.; Moarefi, I.; Kuriyan, J. Crystal structure of the Src family tyrosine kinase Hck. *Nature* **1997**, *385*, 602−609.
(45) Hammerman, P. S.; Fox, C. J.; Birnbaum, M. J.; Thompson, C. B. The Pim and Akt oncogenes are independent regulators of hematopoietic cell growth and survival. *Blood*, in press.
(46) Lopez-Lazaro M. Flavonoids as anticancer agents: structure-activity relationship study. *Curr. Med. Chem.: Anti-Cancer Agents* **2002**, *2*, 691−714.
(47) Akiyama, T.; Ishida, J.; Nakagawa, S.; Ogawara, H.; Watanabe, S.; Itoh, N.; Shibuya, M.; Fukami, Y. Genistein, a specific inhibitor of tyrosine-specific protein kinases. *J. Biol. Chem*. **1987**, *262*, 5592−5595.
(48) Birt, D. F.; Hendrich, S.; Wang, W. Dietary agents in cancer prevention: flavonoids and isoflavonoids. *Pharmacol. Ther*. **2001**, *90*, 157−177.
(49) Lu, H.; Chang, D. J.; Baratte, B.; Meijer, L.; Schulze-Gahmen, U. Crystal structure of a human cyclin-dependent kinase 6 complex with a flavonol inhibitor, fisetin. *J. Med. Chem*. **2005**, *48*, 737−743.
(50) Hanke, J. H.; Gardner, J. P.; Dow, R. L.; Changelian, P. S.; Brissette, W. H.; Weringer, E. J.; Pollok, B. A.; Connelly, P. A. Discovery of a novel, potent, and Src family-selective tyrosine kinase inhibitor. Study of Lck- and FynT-dependent cell activation. *J. Biol. Chem*. **1996**, *271*, 695−701.
(51) Schindler, T.; Sicheri, F.; Pico, A.; Gazit, A.; Levitzki, A.; Kuriyan, J. Crystal structure of Hck in complex with a Src family-selective tyrosine kinase inhibitor. *Mol. Cell* **1999**, *3*, 639−648.
(52) Peat, A. J.; Boucheron, J. A.; Dickerson, S. H.; Garrido, D.; Mills, W.; Peckham, J.; Preugschat, F.; Smalley, T.; Schweiker, S. L.; Wilson, J. R.; Wang, T. Y.; Zhou, H. Q.; Thomson, S. A. Novel pyrazolopyrimidine derivatives as GSK-3 inhibitors. *Bioorg. Med. Chem. Lett*. **2004**, *14*, 2121−2125.
(53) Markwalder, J. A.; Arnone, M. R.; Benfield, P. A.; Boisclair, M.; Burton, C. R.; Chang, C. H.; Cox, S. S.; Czerniak, P. M.; Dean, C. L.; Doleniak, D.; Grafstrom, R.; Harrison, B. A.; Kaltenbach, R. F., 3rd; Nugiel, D. A.; Rossi, K. A.; Sherk, S. R.; Sisk, L. M.; Stouten, P.; Trainor, G. L.; Worland, P.; Seitz, S. P. Synthesis and biological evaluation of 1-aryl-4,5-dihydro-1H-pyrazolo[3,4-d]pyrimidin-4-one inhibitors of cyclin-dependent kinases. *J. Med. Chem*. **2004**, *18*, 5894−5911.
(54) Moravcova, D.; Krystof, V.; Havlicek, L.; Moravec, J.; Lenobel, R.; Strnad, M. Pyrazolo[4,3-d]pyrimidines as new generation of cyclin-dependent kinase inhibitors. *Bioorg. Med. Chem. Lett*. **2003**, *13*, 2989−2992.
(55) Williamson, D. S.; Parratt, M. J.; Bower, J. F.; Moore, J. D.; Richardson, C. M.; Dokurno, P.; Cansfield, A. D.; Francis, G. L.; Hebdon, R. J.; Howes, R.; Jackson, P. S.; Lockie, A. M.; Murray, J. B.; Nunns, C. L.; Powles, J.; Robertson, A.; Surgenor, A. E.; Torrance, C. J. Structure-guided design of pyrazolo[1,5-a]pyrimidines as inhibitors of human cyclin-dependent kinase 2. *Bioorg. Med. Chem. Lett*. **2005**, *15*, 863−867.
(56) Fraley, M. E.; Hoffman, W. F.; Rubino, R. S.; Hungate, R. W.; Tebben, A. J.; Rutledge, R. Z.; McFall, R. C.; Huckle, W. R.; Kendall, R. L.; Coll, K. E.; Thomas, K. A. Synthesis and initial SAR studies of 3,6-disubstituted pyrazolo[1,5-a]pyrimidines: a new class of KDR kinase inhibitors. *Bioorg. Med. Chem. Lett*. **2002**, *12*, 2767−2770.
(57) Anderson, M.; Beattie, J. F.; Breault, G. A.; Breed, J.; Byth, K. F.; Culshaw, J. D.; Ellston, R. P.; Green, S.; Minshull, C. A.; Norman, R. A.; Pauptit, R. A.; Stanway, J.; Thomas, A. P.; Jewsbury, P. J. Imidazo[1,2-a]pyridines: a potent and selective class of cyclin-dependent kinase inhibitors identified through structure-based hybridisation. *Bioorg. Med. Chem. Lett*. **2003**, *13*, 3021−3026.
(58) Hamdouchi, C.; Zhong, B.; Mendoza, J.; Collins, E.; Jaramillo, C.; De Diego, J. E.; Robertson, D.; Spencer, C. D.; Anderson, B. D.; Watkins, S. A.; Zhang, F.; Brooks, H. B. Structure-based design of a new class of highly selective aminoimidazo[1,2-a]-pyridine-based inhibitors of cyclin dependent kinases. *Bioorg. Med. Chem. Lett*. **2005**, *17*, 1943−1947.
(59) Byth, K. F.; Cooper, N.; Culshaw, J. D.; Heaton, D. W.; Oakes, S. E.; Minshull, C. A.; Norman, R. A.; Pauptit, R. A.; Tucker, J. A.; Breed, J.; Pannifer, A.; Rowsell, S.; Stanway, J. J.; Valentine, A. L.; Thomas, A. P. Imidazo[1,2-b]pyridazines: a potent and selective class of cyclin-dependent kinase inhibitors. *Bioorg. Med. Chem. Lett*. **2004**, *14*, 2249−2252.

JM0504858